Connecting Galaxy Evolution, Star Formation and the X-ray Background

D. R. Ballantyne[1], J. E. Everett and N. Murray

Canadian Institute for Theoretical Astrophysics, McLennan Labs, 60 St. George Street, Toronto, Ontario, Canada M5S 3H8

ballantyne, everett, murray@cita.utoronto.ca

ABSTRACT

As a result of deep hard X-ray observations by *Chandra* and *XMM-Newton* a significant fraction of the cosmic X-ray background (CXRB) has been resolved into individual sources. These objects are almost all active galactic nuclei (AGN) and optical followup observations find that they are mostly obscured Type 2 AGN, have Seyfert-like X-ray luminosities (i.e., $L_X \sim 10^{43-44}$ ergs s^{-1}), and peak in redshift at $z \sim 0.7$. Since this redshift is similar to the peak in the cosmic star-formation rate, this paper proposes that the obscuring material required for AGN unification is regulated by star-formation within the host galaxy. We test this idea by computing CXRB synthesis models with a ratio of Type 2/Type 1 AGN that is a function of both z and 2–10 keV X-ray luminosity, L_X. The evolutionary models are constrained by parameterizing the observed Type 1 AGN fractions from the recent work by Barger et al. The parameterization which simultaneously best accounts for Barger's data, the CXRB spectrum and the X-ray number counts has a local, low-L_X Type 2/Type 1 ratio of 4, and predicts a Type 2 AGN fraction which evolves as $(1+z)^{0.3}$. Models with no redshift evolution yielded much poorer fits to the Barger Type 1 AGN fractions. This particular evolution predicts a Type 2/Type 1 ratio of 1–2 for $\log L_X > 44$, and thus the deep X-ray surveys are missing about half the obscured AGN with these luminosities. These objects are likely to be Compton thick. The parameterization also predicts a covering fraction approaching unity at $z \sim 1$ and $\log L_X \sim 41.5$ which would be very difficult to explain using a simple unevolving torus model. Overall, these calculations show that the current data strongly supports a change to the AGN unification scenario where the obscuration is connected with star formation in the

[1]Current address: Department of Physics, University of Arizona, 1118 East 4th Street, Tucson, AZ 85721; drb@physics.arizona.edu

host galaxy rather than a molecular torus alone. The evolution of the obscuration implies a close relationship between star formation and AGN fueling, most likely due to minor mergers or interactions.

Subject headings: galaxies: active — galaxies: evolution — galaxies: formation — galaxies: Seyfert — X-rays: diffuse background

1. Introduction

In recent years, theories of the formation and evolution of active galactic nuclei (AGN) have been dominated by a simple geometric unification model (Antonucci 1993). It is envisaged that an optically thick obscuring torus lies between the broad-line and narrow-line regions at a distance of ~ 1 pc from the central black hole, and the orientation to the line-of-sight of this torus is the dominant parameter in determining the observational properties of an AGN. The opening angle of the torus is such that it blocks the view of the optical/UV continuum and broad-line region for most observers, and therefore accounts for the observed dominance of narrow-line AGN (Type 2s) over broad-line AGN (Type 1s) in the local universe (Maiolino & Rieke 1995). The torus will also produce absorption in the X-ray band, and, indeed X-ray observations generally show that optical Type 2 AGN exhibit more soft X-ray absorption than Type 1 objects (Bassani et al. 1999; Risaliti, Maiolino & Salvati 1999). However, there are exceptions to this rule (e.g., Panessa & Bassani 2002; Barcons, Carrera & Ceballos 2003) and rapid absorption variability observed in some local AGN (Risaliti, Elvis & Nicastro 2002; Risaliti et al. 2005) indicate that refinements to the toroidal unification picture are required.

The geometric AGN unification model is also an important component in explaining the shape of the cosmic X-ray background (CXRB; Giacconi et al. 1962) at energies > 1 keV. Between 1 and 20 keV the CXRB can be described by a power-law with a photon-index of $\Gamma \approx 1.4$ (Kushino et al. 2002; Lumb et al. 2002; De Luca & Molendi 2004), while most unobscured AGN are observed to have $\Gamma = 1.9$ (after taking into account the effects of Compton reflection; Mushotzky, Done & Pounds 1993). It was therefore postulated that the spectrum of the CXRB can be built up by summing the spectra of many obscured AGN over a distribution in redshift, luminosity and absorbing column density $N_{\rm H}$ (Setti & Woltjer 1989; see Gilli 2004 for a recent review). This picture has now been largely confirmed by very deep X-ray observations by *Chandra* and *XMM-Newton* that have resolved 50–90% of the background below 10 keV into individual sources (Mushotzky et al. 2000; Brandt & Hasinger 2005; Worsley et al. 2005). Interestingly, optical followup of these objects have shown that they mostly reside at redshifts $0.7 \lesssim z \lesssim 1.1$ (e.g., Tozzi et al. 2001; Barger et

al. 2002, 2005) and have X-ray luminosities typical of Seyfert galaxies ($L_X \sim 10^{43}$ erg s^{-1}). This is in contrast with the predictions of the earlier synthesis models (Madau, Ghisellini & Fabian 1994; Comastri et al. 1995; Gilli, Risaliti & Salvati 1999; Pompilio, La Franca & Matt 2000; Gilli, Salvati & Hasinger 2001) which were based on the local Type 2/Type 1 ratio, and thus expected a large number of Type 2 quasars — obscured high luminosity objects ($L_X > 10^{45}$ erg s^{-1}) — at redshifts $z \sim 1-2$. Indeed, X-ray luminosity functions measured by Barger et al. (2005), Ueda et al. (2003), and Hasinger, Miyaji & Schmidt (2005) show that at $z \lesssim 1$ the space density of AGN is dominated by moderate-luminosity Seyfert galaxies. Treister et al. (2004) argue, however, that an unevolving unified model (i.e., a torus) is still consistent with the data if the deep surveys are subject to significant selection effects (see also Treister & Urry 2005).

At the same time as the CXRB was being revealed, observations by the *Hubble Space Telescope* showed a remarkable connection between the mass of the supermassive black hole in the centers of local, inactive galaxies and the mass of the galactic bulge (Maggorian et al. 1998; Ferrarese & Merritt 2000; Gebhardt et al. 2000; Tremaine et al. 2002). It now seems clear that the growth of both the central black hole and galaxy must be connected in a fundamental way, and that feedback from the accreting black hole and/or star forming-regions have a significant impact on the structure of the bulge (e.g., Silk & Rees 1998; Fabian 1999; Kaufmann & Haehnelt 2000; Wyithe & Loeb 2003; Murray, Quataert & Thompson 2005; Di Matteo, Springel & Hernquist 2005). While the connection between star-formation and black hole accretion has long been suspected based on observations of local Seyfert 2s (e.g., Cid Fernandes et al. 2001; Joguet et al. 2001), further evidence has been provided by the redshift distribution of the *Chandra* CXRB sources (Barger et al. 2003; Zheng et al. 2004; Szokoly et al. 2004), which peaks at about the same redshift as the cosmic star formation rate (Madau et al. 1996; Chary & Elbaz 2001; Le Floc'h et al. 2005). More recent CXRB synthesis models which allow Type 2 objects to separately evolve as infrared-bright star-forming galaxies (Franceschini et al. 2002; Gandhi & Fabian 2003) can reproduce the low-z peak in the redshift distribution, but seem to overpredict the number of obscured AGN at $z < 1$ (Gilli 2004).

Recent observations are providing significant pressure on the basic assumption that an unevolving unified model can be applied for all AGN at all redshifts. The comprehensive optical follow-up work of Barger et al. (2005) on X-ray deep fields provides compelling evidence that the fraction of Type 1 objects increases significantly with luminosity even at redshifts as low as $z = 0.1$–0.4. The large numbers of obscured Seyferts at $z \lesssim 1$ indicate galaxy formation and evolution is still ongoing at this era, but is evidently different than the earlier quasar epoch which seems to have a much smaller fraction of obscured AGN (Perola et al. 2004; Szokoly et al. 2004). Perhaps there are large numbers of Type 2 quasars which have

been missed in the deep surveys due to selection effects (i.e., buried quasars which release the majority of their bolometric luminosity in the infrared; Hines et al. 1995), a possibility that future *Spitzer* surveys should elucidate[1]. Alternatively, the lack of Type 2 quasars may be explained by invoking the 'receding torus' model (Lawrence 1991; Simpson 2005), where, because of the effects of dust sublimation, the inner radius of the torus is increased at higher luminosity. Another possibility is that radiation pressure flattens the torus in high luminosity objects (Königl & Kartje 1994). Both these explanations, since they assume no connection between the AGN and the host galaxy, should be independent of redshift, but Figure 19 in the paper by Barger et al. (2005) also shows evidence that the broad-line AGN fraction decreases with redshift at a given luminosity. These authors find that at the redshift where the bulk of the CXRB is produced ($z \sim 0.7 - 1$), the Type 1 fraction at a luminosity of 10^{43} erg s^{-1} is only $\sim$20% as compared to 70–80% at $z = 0.1 - 0.4$. In addition, the low redshift ($z < 0.15$) optical Type 1 and 2 luminosity functions constructed by Hao et al. (2005) from nearly 3000 AGN in the Sloan Digital Sky Survey find a Type 2/Type 1 ratio of approximately unity at low Seyfert luminosities, with Type 1s dominating at higher luminosities (see also Heckman et al. 2005). These results all imply that the obscuring material responsible for blocking the AGN continuum in Seyfert 2s evolves with redshift, as well as luminosity. Moreover, if the Sloan results are accurate the absorbing medium must evolve so that it increases its covering fraction by a factor of 3–4 from $z \sim 0$ to $z \sim 1$. This evolution exactly tracks that of the star formation rate in the universe.

The central idea proposed here is that the obscuration important for providing the correct shape of the CXRB is regulated by and controlled via active star-formation within the galaxy. The actual processes responsible for the obscuration are unknown, but it may be associated with star-formation on many-hundred pc scales, or be brought in closer to the nucleus by a starburst disk (Thompson, Quataert & Murray 2005). Thus, the Type 2/Type 1 ratio does evolve with redshift and peaks at $z \sim 1$, where both the star-formation rate is a maximum and the majority of the obscured AGN discovered by the deep surveys are found. Similar ideas have been discussed before (Fabian et al. 1998; Franceschini et al. 1999), but here we use the latest observational constraints on the CXRB spectrum, source number counts and Type 2/Type 1 ratio ($\equiv R$) to determine what kind of AGN evolution is possible and if it is consistent with the above hypothesis.

We begin by describing in the next section the calculation of the CXRB spectrum and number counts, including assumptions on the AGN spectral model and evolution of R. Sec-

[1]Although very recent *Spitzer* results (Rigby et al. 2005) have shown that many of the optically faint X-ray sources, while at higher redshift, still have Seyfert luminosities and therefore do not contribute to evolution of the quasars.

tion 3 presents the results of the computations and compares them against the data. We discuss the implications of the results for the unified model and models of galaxy formation/evolution in Sect. 4, and then present our conclusions in Sect. 5.

This paper assumes the standard *WMAP* and *Boomerang* Λ-dominated cosmology: $H_0 = 70$ km s^{-1} Mpc^{-1}, $\Omega_\Lambda = 0.7$, and $\Omega_m = 0.3$ (Spergel et al. 2003; MacTavish et al. 2005).

2. CXRB Synthesis Model

2.1. Formalism

The calculation of the CXRB spectrum and number counts follows the standard method outlined in earlier works (e.g., Comastri et al. 1995; Pompilio et al. 2000).

The spectral intensity of the CXRB (in keV cm^{-2} s^{-1} keV^{-1} str^{-1}) at energy E is given by

$$I(E) = \frac{c}{H_0} \int_{z_{\rm min}}^{z_{\rm max}} \int_{\log L_X^{\rm min}}^{\log L_X^{\rm max}} \frac{d\Phi(L_X, z)}{d\log L_X} \frac{S_E(L_X, z) d_l^2}{(1+z)^2(\Omega_m(1+z)^3 + \Omega_\Lambda)^{1/2}} d\log L_X dz, \quad (1)$$

where $d\Phi(L_X, z)/d\log L_X$ is the X-ray luminosity function for AGN (in Mpc^{-3}), $S_E(L_X, z)$ is the absorbed observed-frame spectrum of an AGN (in keV cm^{-2} s^{-1} keV^{-1}) with intrinsic luminosity L_X at redshift z, and d_l is the luminosity distance to redshift z:

$$d_l = (1+z)\frac{c}{H_0} \int_0^z \frac{dz'}{(\Omega_m(1+z')^3 + \Omega_\Lambda)^{1/2}}. \quad (2)$$

A similar expression is used to calculate the number of sources per square degree with flux (defined in some energy band) greater than F, $N(>F)$

$$N(>F) = \frac{K_{\rm str}^{\rm deg} c}{H_0} \int_{z_{\rm min}}^{z_{\rm max}} \int_{\max(\log L_X^{\rm min}, \log L_X^F)}^{\log L_X^{\rm max}} \frac{d\Phi(L_X, z)}{d\log L_X} \frac{d_l^2}{(1+z)^2(\Omega_m(1+z)^3 + \Omega_\Lambda)^{1/2}} d\log L_X dz, \quad (3)$$

where $K_{\rm str}^{\rm deg} = 3 \times 10^{-4}$ is the conversion factor from str^{-1} to degrees^{-2}, $\log L_X^F$ is the rest-frame luminosity corresponding to observed-frame flux F at redshift z.

2.2. Ingredients

To generate a CXRB model with the above equations, a number of key ingredients must be specified.

2.2.1. The Luminosity Function

For the normalization and evolution of the space density of AGN, we use the hard X-ray luminosity function (HXLF) of Ueda et al. (2003). It is defined for the absorption corrected luminosity in the rest-frame 2–10 keV band. As it is absorption-corrected, it describes the density and evolution of all detected AGN, both Type 1 and 2.

Ueda et al. (2003) found that the evolution of the luminosity function was best described using a luminosity-dependent density evolution (LDDE) model such that the lower luminosity objects peaked in density at lower redshift than sources with higher luminosities. In contrast, Barger et al. (2005) found that pure luminosity evolution was the best fit to their hard X-ray luminosity function at $z < 1$. However, recent work by Hasinger et al. (2005) and La Franca et al. (2005) have both found that LDDE best describes AGN evolution from $z \sim 0$ to $z \sim 4 - 5$. In this paper, we assume the LDDE model and parameters of Ueda et al. (2003).

Following Ueda et al. (2003) and Treister & Urry (2005), we take $z_{\rm min} = 0$, $z_{\rm max} = 5$, $\log L_X^{\rm min} = 41.5$, and $\log L_X^{\rm max} = 48$, where from this point on the luminosity L_X refers to 2–10 keV luminosity.

2.2.2. Spectrum

Consistent with using the Ueda et al. (2003) HXLF where there is no distinction between the Type 1 or Type 2 objects, a single spectral model is assumed for all the AGN in the calculation. Shemmer et al. (2005) have recently shown that there is little change in the X-ray spectral shape of AGNs over a large range of luminosity and redshift. The spectrum defined here consists of a power-law with photon-index $\Gamma = 1.9$ and high-energy rollover at 375 keV, augmented by Compton reflection. The PEXRAV model of Magdziarz & Zdziarski (1995) is used to calculate the reflection spectrum with a reflection fraction of unity, solar abundances, and an inclination angle of 63 degrees. This model is very similar to ones assumed in other CXRB synthesis calculations (e.g., Treister & Urry 2005). The spectrum was calculated from 0.1 to 900 keV in 1000 logarithmically spaced steps.

2.2.3. K-correction

The following expression is used to convert from 2–10 keV flux, $F_{2-10\ \mathrm{keV}}$, to luminosity (e.g., Hogg et al. 2002):

$$L_X^{2-10} = \frac{4\pi d_l^2 F_{2-10\ \mathrm{keV}}}{(1+z)}. \tag{4}$$

2.2.4. N_{H} Distribution

As has been standard over the last few years, Type 2 objects are defined here to be those which are seen through columns $\log N_{\mathrm{H}} \geq 22$, with Type 1s being less absorbed. Once the ratio of absorbed to unabsorbed objects (R) is calculated for a given z and L_X (see § 2.3), the N_{H} distribution for the obscured and unobscured AGN must be defined. However, the distribution of absorbing columns for AGN is unknown except for locally, where Risaliti et al. (1999) measured it for nearby luminous Seyfert 2s.

Ten N_{H} bins are defined in the calculation: $\log N_{\mathrm{H}} = 20, 20.5, \ldots, 24, 24.5$. The implicit assumption is that objects which are severely Compton-thick with $\log N_{\mathrm{H}} \geq 25$ will not significantly contribute to the observed CXRB. In lieu of any other information, we first make the simplest choice and assume a flat N_{H} distribution for both Type 1 and Type 2 sources. Computations were also performed with the Risaliti et al. (1999) distribution where 75% of all Type 2s have $\log N_{\mathrm{H}} \geq 23$ and half are Compton thick.

For $\log N_{\mathrm{H}} \leq 23$, the solar abundance photoelectric cross-sections of Morrison & McCammon (1983) are used to modify the spectrum. At higher columns, where Compton scattering becomes important within the absorber, we extracted the results plotted by Matt, Pompilio & La Franca (1999) and divided them by their incident spectrum ($\Gamma = 2$ power-law with cutoff energy of 500 keV) to obtain the absorption/transmission curve in our energy range. We then applied the appropriate curve to our model spectrum to account for Compton-thick absorbing columns. The effects of correctly including the absorption and transmission properties of Compton-thick columns are illustrated in Figure 1 where we reproduce the results of Treister & Urry (2005). Including the proper treatment of Compton thick absorbers produced a poorer fit for this set of parameters.

2.3. The Evolving Type 2/Type 1 Ratio

The central hypothesis in this work is that the Type 2/Type 1 ratio, R, will increase with redshift until $z \sim 1$. In addition, R will decrease with L_X as seen in many recent

observational campaigns. Since the leading explanations for this effect are based on radiative processes associated with the central engine, we assume that there is no redshift dependence for this L_X-evolution. There is still, however, immense freedom in how the evolution of $R(L_X, z)$ can be described, and as can be seen from previous work (e.g., Gilli et al. 1999; Gandhi & Fabian 2003; Treister & Urry 2005), the CXRB is not very constraining on its own.

We therefore make use of the results presented by Barger et al. (2005) in their Figure 19 which shows the observed fraction of Type 1 objects as a function of 2–8 keV luminosity in three different redshift bins: $0.1 - 0.4$, $0.4 - 0.8$, and $0.8 - 1.2$. While the exact parameterization of $R(L_X, z)$ remains unconstrained, Barger's data provides landmarks to which the model can be pinned. Ideally, we would be able to compute the Type 1 fraction from a self-consistent model of star formation and black hole growth from redshift 1 to zero. However, such a complicated calculation is not necessary for this study. At this stage, it suffices to determine if redshift evolution of R is needed to explain the observations, and, if so, to quantify the degree of the evolution. We are thus searching for the best description of $R(L_X, z)$ that simultaneously accounts for Barger's data, the CXRB spectrum, and the X-ray number count distributions (in multiple bands).

In practice, we do not compute $R(L_X, z)$, but the related quantities $f_2(L_X, z)$ and $f_1(L_X, z)$, the fraction of Type 2s and Type 1s, respectively. These three parameters are related by

$$f_2(L_X, z) = \frac{R(L_X, z)}{1 + R(L_X, z)} \tag{5}$$

and

$$f_1(L_X, z) = 1 - f_2(L_X, z). \tag{6}$$

Four different parameterizations were used to explore the evolution of the AGN Type 2/Type 1 ratio from $z = 0 - 1$. In addition to the assumptions outlined above, these particular forms were chosen solely as good candidates for accounting for the observed data from Barger et al. (2005), i.e., to smoothly run from 0–1 over the observed range of L_X. The parameterizations are:

$$f_1 = K \exp\left(\frac{L_X}{10^{\beta}(1+z)^{\alpha}}\right), \tag{7}$$

$$f_1 = K(1+z)^{-\alpha}\left(\frac{L_X}{10^{41.5}}\right)^{\beta}, \tag{8}$$

$$f_2 = K(1+z)^{\alpha}(\log L_X)^{-\beta}, \tag{9}$$

and

$$f_2 = K(1+z)^{\alpha}\cos^2\left(\frac{\log L_X - 41.5}{\beta}\right). \tag{10}$$

Aside from α and β the only other free parameter is the normalization K. This is set by defining R at $z = 0$ and $\log L_X = 41.5$, denoted by R_0. At redshifts ≥ 1 the fractions f_2 or f_1 are fixed at their $z = 1$ values, mimicking the roughly flat star-formation rate during this era (Chary & Elbaz 2001). If the value of f_1 or f_2 ever became negative or > 1 then it was forced to zero or one, respectively.

For every $R_0 = 1, 2, \ldots, 9, 10$, we search for the best α and β in each of the four parameterizations by χ^2 fitting to the Barger data. Equations 7-10 are evaluated at the midpoints of the three redshift bins used by Barger et al. (2005), namely, $z = 0.25, 0.6$ and 1.0. The values of L_X are taken directly from the Barger data, and we ignore the small difference between 2–8 keV and 2–10 keV luminosities (17% when $\Gamma = 1.9$). The errorbars on each datapoint are obtained from their plot. If only one errorbar is visible then we assume they are symmetric. The $\log L_X \approx 42.8$ data point in the $z = 0.8 - 1.2$ bin and the $\log L_X \approx 42.3$ point in the $z = 0.4 - 0.8$ bin are omitted in the χ^2 calculation because they were an upper-limit or had very small errorbars. The χ^2 calculation took into account the data from all three redshift bins, thus we are searching for the model that can best account for the observed redshift and luminosity evolution over the entire range in z and L_X. There are 13 data points and 2 free parameters, resulting in 11 degrees of freedom (d.o.f.).

The minimum χ^2 is searched for by iterating over a large α and β parameter space. Once the best fit α and β are known for each R_0, the evolution equations 7-10 are inserted into the CXRB machinery described in § 2.1. Predictions of the CXRB spectrum and number counts are then computed for the different evolutions and compared with the observations. As in previous work (Gandhi & Fabian 2003), the normalization of the predicted spectrum is multiplied by a constant in order to fit the observed data (whose normalization is also uncertain; De Luca & Molendi 2004).

3. Results

3.1. z and L_X evolution

The best fit values of α and β for all four evolution models are shown in Table 1, along with the computed χ^2 and the corresponding null-hypothesis probability P_{χ^2}. The power-law parametrization (Eq. 8) seems to provide the best fit to the Barger data for every assumed R_0, with some very low values of χ^2 obtained when $R_0 > 4$. The cosine model (Eq. 10) is the next best parameterization, with good fits obtained for every $R_0 > 1$. The exponential model (Eq. 7) only finds very good fits at large values of R_0, while the $\log L_X$ power-law model (Eq. 9) results in $\chi^2/\text{d.o.f.} \gtrsim 1$.

In order to use these values of α and β to predict the CXRB properties, an $N_{\rm H}$ distribution must be assumed. In § 3.1.1 we use a simple prescription where the columns of Type II AGN are spread uniformly between $\log N_{\rm H} = 22$ and 24.5, and similarly for Type I AGN between $\log N_{\rm H} = 20$ and 21.5. Results assuming the Risaliti et al. (1999) $N_{\rm H}$ distribution are presented in § 3.1.2.

3.1.1. Simple $N_{\rm H}$ Distribution

While the normalization of the CXRB is still uncertain (De Luca & Molendi 2004), the spectral slope is well constrained to be $\Gamma \approx 1.4$ above 1 keV (e.g. Kushino et al. 2002). To provide a quantitative estimate of how well our evolutionary models fit the CXRB spectrum, we computed Γ between 1 and 10 keV and the results are listed in the penultimate column of Table 1. Interestingly, the power-law evolutionary model, which gives the best fit to the Barger data, fails badly in recovering the shape of the CXRB spectrum. This is illustrated in Fig. 2 for the case of $R_0 = 6$. We find that there are far too few absorbed sources in this model to successfully account for the shape of the observed CXRB. In fact, we find that, in general, the closer one fits the Barger et al. (2005) data, the poorer the fit to the CXRB spectrum.

The best match to the observed CXRB was found with the $\log L_X$ power-law model (Eq. 9), the one that provided decent, but not spectacular, fits to Barger's data ($P_{\chi^2} \sim 0.2 - 0.4$). Figure 3 plots the results from this evolutionary model assuming $R_0 = 1$, the value pointed to by the recent Sloan analysis (Hao et al. 2005; Heckman et al. 2005). This model can successfully reproduce the properties of both the CXRB spectrum and the number counts, but produces a very poor fit to Barger's Type 1 fractions. Indeed, the model, which requires very strong z evolution to fit the CXRB, predicts that the X-ray surveys are missing many low-L_X Type 1 objects at $z \leq 0.6$ as well as many high-L_X absorbed objects at all z, both by factors of 2–5. As a consequence, Type 2 quasars are predicted to be 4–5 times as numerous as Type 1 quasars at $z \gtrsim 1$, a result that does not seem to be borne out by recent observations (Martínez-Sansigre et al. 2005).

Figure 4 represents a compromise solution. Here, we plot the results of the $\log L_X$ power-law model with $R_0 = 4$, similar to the classic ratio of Maiolino & Rieke (1995). Table 1 tells us that the fit to Barger's data is adequate, and that the 1–10 keV slope is $\Gamma = 1.418$, close to the observed value. The predicted number counts seem consistent with the observations from the *Chandra* deep fields. In this case, the prediction is that the X-ray surveys are missing $\sim 50\%$ of the absorbed high-L_X objects. In Figure 5 we plot contours of $R(L_X, z)$ predicted by this evolution model between $z = 0 - 2$. The ratio of Type 2 to Type 1 quasars

is predicted to be between 1 and 2, more consistent with the recent observational limits. The model also predicts that low-L_X AGN at high z will almost always be completely obscured, a situation that would be difficult to obtain for a standard unevolving circumnuclear AGN torus.

3.1.2. The Risaliti et al. (1999) $N_{\rm H}$ Distribution

In a survey of local Seyfert 2 galaxies, Risaliti et al. (1999) found that $\sim 75\%$ had $\log N_{\rm H} \geq 23$, and about half were Compton thick. We computed CXRB models using the same values of α and β as in the previous section, but now assuming the Risaliti et al. (1999) $N_{\rm H}$ distribution for Type 2 objects (the $N_{\rm H}$ distribution for Type 1 AGN was unchanged). This results in 50% more Compton thick objects than with the previous flat distribution.

The photon-index between 1 and 10 keV for the predicted CXRB spectra for these models, denoted $\Gamma_{1-10}^{\rm Risaliti}$, is listed in the final column of Table 1. In general, there are only slight differences in the spectral slopes from the two $N_{\rm H}$ distributions. For those cases when the Barger data is fit very well and Type 2 AGNs are not dominant then the spectral slope is slightly softer than before. This is because more absorbed AGN are Compton thick and thus have little effect on the spectral shape below 10 keV (see Fig. 6). However, if Type 2 AGNs are the dominant population, as in cases which fit the Barger data poorly, the additional Compton thick sources do slightly harden the 1–10 keV spectral slope.

While the effect on spectral shape below 10 keV may be minimal, the additional Compton thick AGN will significantly influence the predicted spectrum at higher energies, particularly when Type 2 objects are dominant. This is illustrated in Figures 7 and 8 where we plot the predicted CXRB spectrum and number count distributions for the $\log L_X$ power-law model when $R_0 = 1$ and 4, respectively. These plots are the equivalent of ones from Figs. 3 and 4, but with the Risaliti et al. (1999) $N_{\rm H}$ distribution. One can clearly see that the large number of Compton thick sources in the Risaliti distribution provides a much better fit to the peak of the observed CXRB spectrum at 40–50 keV than the simple $N_{\rm H}$ model used previously. However, the additional absorption also impacts the number counts, and we find that in both the $R_0 = 1$ and 4 models, the 2–8 keV number counts underpredict the observations at all fluxes. These results imply that additional Compton thick sources above the simple $N_{\rm H}$ model are necessary to best fit the CXRB spectrum, but that the Risaliti et al. (1999) distribution cannot hold at all z and L_X.

3.2. Is z evolution required?

The above results show that we have managed to account for the Barger et al. (2005) data, the CXRB spectrum, and the X-ray number counts with a model that assumes z evolution of R. However, it is not clear if the data require such evolution; indeed, successful fits of the CXRB spectrum and number counts have been obtained with no z evolution of R (Gandhi & Fabian 2003; Treister & Urry 2005). The Barger data provides an additional constraint, so to test if z evolution is needed to fit these data, we removed the z-dependence from equations 7-10 and performed new χ^2 fitting for the luminosity parameter β. The results are shown in Table 2 and should be compared with the results in Table 1. In every case but one, the fit with no redshift dependence is worse, often by a large amount, than the corresponding one with z dependence. In fact, there are only 18 models with no z-dependence that resulted in $P_{\chi^2} > 0.1$, as compared to 33 when redshift evolution was allowed. In addition, when adequate fits were obtained they required $R_0 > 6$, which reduces their plausibility. Our conclusion is that, to the extent that the Barger et al. (2005) data is an accurate depiction of R from $z = 0 - 1$, then the data is best described by a model that includes redshift evolution of the Type 2/Type 1 AGN ratio. Moreover, if the Sloan data are accurate and $R_0 \approx 1$ then strong redshift evolution is required to fit the CXRB.

3.3. Luminosity-dependent z evolution

The LDDE models of the X-ray AGN luminosity function (Ueda et al. 2003; Hasinger et al. 2005) indicate that the most massive black holes, typically responsible for luminous quasars, form earlier than less massive black holes which power Seyfert galaxies (i.e., anti-hierarchal formation; Merloni 2004; Tamura, Ohta & Ueda 2006). Also, radiative and wind-driven feedback will be more important for luminous AGNs and will combat the tendency for increasing obscuration. Thus, it may be possible that the redshift evolution of the Type 2/Type 1 AGN ratio may also depend on luminosity. To test this, we allow the α parameter in our evolutionary models (Eqs. 7-10) to be dependent on $\log L_X$ via a simple linear relation: $\alpha(L_X) = m \log L_X + b$. The slope and intercept of this line was determined by fixing α at $\log L_X = 41.5$, denoted $\alpha_{41.5}$, to the appropriate value in Table 1, and fit the Barger data for $\alpha_{43.5}$, the value of α at $\log L_X = 43.5$, along with β. The results of this exercise are shown in Table 3. In all cases, the quality of the fits are equal to or better than the ones where α was independent of L_X, although the two models are statistically identical.

In terms of the direction of the L_X-dependence, the results are inconclusive. The exponential evolutionary model prefers a positive slope (i.e., the covering factor increases faster with z at higher L_X) when $R_0 < 5$, and zero slope in all other cases. The power-law model

gives a negative slope (slower increase of the covering factor with z at higher L_X) for $R_0 < 8$ and a positive one for $R_0 \geq 8$. The cosine model seems to vary from zero slope to slightly positive, but the $\log L_X$ power-law model consistently produces a negative slope, often with $\alpha_{43.5} = 0.0$, which implies *negative* evolution of the covering factor with z for large L_X AGN. Our conclusion is that the available data is not constraining enough to presently determine if there is a luminosity dependence to the redshift evolution of R. There is tentative evidence that a negative slope is preferred, which, as mentioned above, indicates that obscuration increases more slowly with z for more luminous AGNs. This can be understood if the star-formation rate in these more luminous AGNs does not increase very rapidly from $z = 0 - 1$.

4. Discussion

In the previous section, we found that an evolving Type 2/Type 1 AGN ratio, $R(L_X, z)$, determined by fitting the Type 1 ratios observed by Barger et al. (2005) can account for the CXRB spectrum and number counts. Indeed, models with no z dependence provide significantly worse fits to Barger's data. Here, we discuss the impact of this result on the observations, AGN unification and evolution, as well as the connection to galaxy evolution.

4.1. Implications for X-ray and Optical Observations

Section 3 presented moderately strong evidence for redshift evolution of the obscuring medium around an AGN, but the strength of that evolution depends on the assumption on what the local Type 2/Type 1 ratio is at low L_X. On one extreme, if we accept the Sloan results that $R_0 = 1$ (Hao et al. 2005; Heckman et al. 2005), then very strong z evolution is needed ($f_2 \propto (1+z)^{0.9}$) in order to account for the CXRB spectrum (Figs. 3 and 7). However, this parameterization completely fails to fit the Type 1 ratios observed by Barger et al. (2005), requiring the X-ray surveys to miss many low-luminosity unobscured sources and high luminosity obscured AGN. On the other hand, models which best fit the Barger data (e.g., Figs. 2 and 6) cannot reproduce the shape of the CXRB spectrum for any R_0 — there are too many unobscured AGN.

We conclude that the best compromise solution is the $R_0 = 4$ model shown in Figs. 4 and 8. This parameterization provides an adequate fit to the Barger data and a good match to the observed shape of the CXRB spectrum and X-ray number counts. It predicts a redshift evolution of the Type 2 AGN fraction of $f_2 \propto (1+z)^{0.3}$. We prefer this solution

over the $R_0 = 1$ Sloan-inspired model because the value of R_0 is consistent with earlier work (Maiolino & Rieke 1995) and it requires fewer missing obscured sources at higher z. The implication is that the Sloan work is missing local obscured sources. These could be AGN whose narrow-line regions are obscured and reddened, and therefore only appear as AGN in the X-ray (i.e., X-ray Bright Optically Inactive Galaxies or elusive AGN; Maiolino et al. 2003; Comastri et al. 2002; Georgantopolous & Georgakakis 2005). Future observational work is required to accurate measure the local value of R over a range in L_X. This type of measurement is vital to the understanding of AGN and galaxy evolution – only when the local Type 2/Type 1 ratio is well known can the amount of evolution be determined.

As described by Brandt & Hasinger (2005), it is likely that the deep X-ray surveys are missing heavily obscured AGN, especially ones that are Compton thick. Evidence for this can be seen in the hard X-ray number counts, which have yet to exhibit a turnover (Rosati et al. 2002), and the stacking analysis of Worsley et al. (2005), who shows that the CXRB may only be ~ 50 % resolved at ~ 10 keV. We propose that the missing obscured AGN predicted by the evolution model will mostly be Compton thick, but that the Type 2/Type 1 ratio will only be $\sim 1 - 2$ at higher AGN luminosities (Fig. 5).

Comparing the results of the CXRB model between a simple uniform $N_{\rm H}$ distribution and the Risaliti et al. (1999) one, where half of the Seyfert 2s are Compton thick, showed that additional Compton thick sources over the uniform model are needed to improve the fit to the CXRB spectrum at $\sim 40 - 50$ keV. However, the Risaliti et al. (1999) ratio is too large to hold in general, because the 2–8 keV number counts are significantly underpredicted. Similar to R, the fraction of Compton-thick Seyfert 2s is likely to be a function of z and L_X. Thus, measurements of the $N_{\rm H}$ distribution at different redshifts and luminosities are needed to accurately constrain the predictions of CXRB synthesis models. A focusing hard X-ray instrument, such as *NuStar*[2], is necessary to discover and trace the evolution of the Compton thick AGN population.

4.2. AGN Unification, AGN Evolution and Galaxy Evolution

These three topics are discussed together because our results, when combined with recent observational and theoretical work, now show that they are connected and dependent processes. One cannot discuss the formation and evolution of a galaxy without accounting for the growth of its black hole (Kaufmann & Haehnelt 2000). Similarly, we assert that the evolution of AGN and their observational appearance is connected to the evolution of the

[2]http://www.nustar.caltech.edu/

host galaxy.

The fact that the ratio of obscured to unobscured AGN increases with redshift requires a change to the traditional unification paradigm[3]. Since the obscuring medium is changing with z it must be influenced by forces and evolution on the extragalactic scale. The cosmic star formation rate, which peaks at a very similar redshift as R, seems to be the most likely candidate. As star formation increases in a galaxy it signals an increase in the amount of absorbing gas and dust present that can act as an obscuring medium for any AGN. The location of the absorbing material would depend on the location and size of the star forming regions and could exist close to the dust sublimation radius (and thus mimic some properties of an absorbing torus), but could also be spread over a large extent in the inner part of the galaxy (McLeod & Rieke 1995). The idea of an extended, more galactic-scale obscuring medium is consistent with recent infra-red (IR) observations which have pointed out the remarkable similarity in the mid-to-far-IR emission between Seyfert 2s and 1s (Kuraszkiewicz et al. 2003; Lutz et al. 2004), in contrast to the predictions of the simple molecular torus model. Of course, galactic scale obscuration of AGN emission is commonly seen in the X-ray band when observing the massively-star-forming Ultra-Luminous InfraRed Galaxies (ULIRGs; e.g., Iwasawa et al. 2005).

If, as seems to be the case, galactic star formation and AGN activity are related then the question of AGN fueling arises (see recent review by Jogee 2005). At this point it is important to distinguish between high luminosity quasars and lower luminosity Seyferts, which dominate the production of the CXRB. As is well known, quasars peak in density at high redshift ($z \sim 2$), and here interactions between gas-rich disk galaxies are more common (Conselice et al. 2003) and would cause the ignition of a substantial starburst and accretion onto a black hole (e.g., Hopkins et al. 2005). Indeed, only these most luminous AGNs show observational evidence for interactions (Hutchings 1987; Disney et al. 1995; Bahcall et al. 1997; Kirhakos et al. 1999). At lower luminosities there is little observational evidence for Seyfert galaxies being associated with mergers (Laurikainen & Salo 1995; Schmitt 2001; Grogin et al. 2005). Likewise, there is no evidence that the decline in star formation from $z \sim 0.7$ is due to a decrease in major mergers (Bell et al. 2005). Rather, it is possible that at lower redshifts most interactions of a large disk galaxy are with smaller, gas poor satellites (Mihos & Hernquist 1994; Wolf et al. 2005; Waskett et al. 2005) that may trigger an accretion phase onto the black hole, but with a much lower amount of obscuration regulated by the associated star formation. Therefore, it is not valid to apply the results of major merger

[3]However, the basic axiom of the unification model (namely, that all AGN are basically identical at the level of the central engine) is unchanged by this result; only the primary source of the obscuration needs to be altered.

calculations to observations like the CXRB which are dominated by Seyferts.

Depending on the exact nature of the interaction, a number of different obscuration geometries could be set up around the black hole, from a nearby starburst disk to an extended gas/dust lane (cf., Ballantyne, Weingartner & Murray 2003). Also, because fueling a black hole is difficult ('the angular momentum problem'; Jogee 2005), a very long time may pass following the interaction before any gas makes it close enough to the center to be accreted rapidly onto the hole. This delay between the causal event and the resulting AGN activity could mask the cause from observations, particularly if the interaction is weak. Thus, the galaxy may not look like it was disrupted by a merger or interaction, but the resulting star formation and AGN activity could still be ongoing.

The power of the CXRB spectrum and the deep X-ray surveys is that they allow an investigation of the global properties of AGN over cosmic time. We now know that most of the accretion in the Universe is obscured, and that this obscuration evolves similar to the star-formation rate. These facts deepen the connection between star-formation and AGN fueling as well as between black hole growth and galaxy evolution. To fully explore and understand these connections, the sources of the CXRB must be found and investigated in more detail over a range of redshift and luminosity.

5. Conclusions

This paper explored the hypothesis that the obscuration around an AGN evolves with both redshift and luminosity. The motivation behind this idea is that the obscuration is due to star-formation ongoing in the host galaxy. Our conclusions are the following:

- To the extent that the Type 1 AGN fractions observed by Barger et al. (2005) are accurate, redshift evolution of the Type 2/Type 1 AGN (R) to $z \sim 1$ is required to best fit the data.

- The evolutionary model that most successfully reproduced the Barger data, the CXRB spectrum, and the X-ray number counts had $R_0 \approx 4$, consistent with Maiolino & Rieke (1995). The redshift evolution of the Type 2 AGN fraction is $(1+z)^{0.3}$.

- These models imply that the deep X-ray surveys are missing about 50% of obscured AGN with $\log L_X > 44$ at all z. These are likely to be mostly Compton thick.

- Additional Compton-thick sources above the uniform $N_{\rm H}$ distribution improve the fit to the CXRB spectrum. However, applying the Risaliti et al. (1999) distribution, where

50% of all Type 2s are Compton thick, over all L_X and z underpredicts the 2–8 keV number counts. The fraction of Compton thick obscured objects should be less than 50% but will likely vary with z and L_X.

- There are very tentative indications that the covering factor evolves more slowly with z for more luminous AGN.
- A simple, non-evolving torus cannot alone provide the AGN obscuration over all cosmic time, and the shape of the CXRB spectrum is due to obscuration correlated with star-formation within the evolving host galaxy.
- Seyfert galaxies, which dominate the production of the CXRB, are likely fueled by minor mergers or interactions which trigger a star formation event somewhere in the nuclear region. Unlike quasars, there may be a significant delay between the interaction and the subsequent ignition of the AGN.

This research was supported by the Natural Sciences and Engineering Research Council of Canada. The authors thank E. Treister and M. Urry for helpful discussions.

REFERENCES

Antonucci, R., 1993, ARA&A, 31, 473

Bahcall, J.N., Kirhakos, S., Saxe, D.H. & Schneider, D.P., 1997, ApJ, 479, 642

Ballantyne, D.R., Weingartner, J.C. & Murray, N., 2003, A&A, 409, 503

Barcons, X., Carrera, F.J. & Ceballos, M.T., 2003, MNRAS, 339, 757

Barger, A.J., Cowie, L.L., Brandt, W.N., Capak, P., Garmire, G.P., Hornschemeier, A.E., Steffan, A.T. & Wehner, E.H., 2002, AJ, 124, 1839

Barger, A.J., Cowie, L.L., Capak, P., Alexander, D.M., Bauer, F.E., Fernandez, E., Brandt, W.N., Garmire, G.P. & Hornschemeier, A.E., 2003, AJ, 126, 632

Barger, A.J., Cowie, L.L., Mushotzky, R.F., Yang, Y., Wang, W.-H., Steffen, A.T. & Capak, P., 2005, ApJ, 129, 578

Bassani, L., Dadina, M., Maiolino, R., Salvati, M., Risaliti, G., Della Ceca, R., Matt, G. & Zamorani, G., 1999, ApJS, 121, 473

Bell, E.F., et al., 2005, ApJ, 625, 23

Brandt, W.N. & Hasinger, G., 2005, ARA&A, 43, 827

Chary, R. & Elbaz, D., 2001, ApJ, 556, 562

Cid Fernandes, R., Jr., Heckman, T.M., Schmitt, H.R., González Delgado, R.M. & Storchi-Bergmann, T., 2001, ApJ, 558, 81

Comastri, A., Setti, G., Zamorani, G. & Hasinger, G., 1995, A&A, 296, 1

Comastri, A., et al., 2002, ApJ, 571, 771

Conselice, C.J., Bershady, M.A., Dickinson, M. & Papovich, C., 2003, AJ, 126, 1183

De Luca, A. & Molendi, S., 2004, A&A, 419, 837

Di Matteo, T., Springel, V. & Hernquist, L., 2005, Nature, 533, 604

Disney, M.J., et al., 1995, Nature, 376, 150

Fabian, A.C., Barcons, X., Almaini, O. & Iwasawa, K., 1998, MNRAS, 297, L11

Fabian, A.C., 1999, MNRAS, 308, L39

Ferrarese, L. & Merritt, D., 2000, ApJ, 539, L9

Franceschini, A., Hasinger, G., Miyaji, T. & Malquori, D., 1999, MNRAS, 310, L5

Franceschini, A., Braito, V. & Fadda, D., 2002, MNRAS, 335, L51

Gandhi, P. & Fabian, A.C., 2003, MNRAS, 339, 1095

Gebhardt, K., et al., 2000, ApJ, 539, L13

Georgantopolous, I. & Georgakakis, A., 2005, MNRAS, 358, 131

Giacconi, R., Gursky, H., Paolini, F.R. & Rossi, B.B., 1962, Phys. Rev. Lett., 9, 439

Gilli, R., 2004, Advances in Space Research, 34, 2470

Gilli, R., Risaliti, G. & Salvati, M., 1999, A&A, 347, 424

Gilli, R., Salvati, M. & Hasinger, G., 2001, A&A, 366, 407

Grogin, et al., 2005, ApJ, 627, L97

Gruber, D.E., Matteson, J.L., Peterson, L.E. & Jung, G.V., 1999, ApJ, 520, 124

Hao, L., et al., 2005, AJ, 129, 1795

Hasinger, G., Miyaji, T. & Schmidt, M., 2005, A&A, 441, 417

Heckman, T.M., Ptak, A., Hornschemeier, A. & Kauffmann, G., 2005, ApJ, 634, 161

Hines, D.C., Schmidt, G.D., Smith, P.S., Cutri, R.M. & Low, F.J., 1995, ApJ, 450, L1

Hogg, D.W., Baldry, I.K., Blanton, M.R. & Eisenstein, D.J., 2002, preprint (astro-ph/0210394)

Hopkins, P.F., Hernquist, L., Martini, P., Cox, T.J., Roberston, B., Di Matteo, T. & Springel, V., 2005, ApJ, 625, L71

Hutchings, J.B., 1987, ApJ, 320, 122

Iwasawa, K., Sanders, D.B., Evans, A.S., Trentham, N., Miniutti, G. & Spoon, H.W.W., 2005, MNRAS, 357, 565

Jogee, S., 2006, in Physics of Active Galactic Nuclei at All Scales, ed. D. Alloin (New York: Springer), in press (astro-ph/0408383)

Joguet, B., Kunth, D., Melnick, J., Terlevich, R. & Terlevich, E., 2001, A&A, 380, 19

Kauffmann, G. & Haehnelt, M., 2000, MNRAS, 311, 576

Kirhakos, S., Bahcall, J.N., Schneider, D.P. & Kristian, J., 1999, ApJ, 520, 67

Königl, A. & Kartje, J.F., 1994, ApJ, 434, 446

Kuraszkiewicz, J.K., et al., 2003, ApJ, 500, 128

Kushino, A., Ishisaki, Y., Morita, U., Yamasaki, N.Y., Ishida, M., Ohashi, T. & Ueda, Y., 2002, PASJ, 54, 327

La Franca, F., et al., 2005, ApJ, 635, 864

Laurikainen, E. & Salo, H., 1995, A&A, 293, 683

Lawrence, A., 1991, MNRAS, 252, 586

Le Floc'h, E., et al., 2005, ApJ, 632, 169

Lehmer, B.D., et al., 2005, ApJS, 161, 21

Lumb, D.H., Warwick, R.S., Page, M. & De Luca, A., 2002, A&A, 389, 93

Lutz, D., Maiolino, R., Spoon, H.W.W. & Moorwood, A.F.M., 2004, A&A, 418, 465

Madau, P., Ghisellini, G. & Fabian, A.C., 1994, MNRAS, 267, L17

MacTavish, C.J., et al., 2005, ApJ, submitted (astro-ph/0507503)

Madau, P., Ferguson, H.C., Dickinson, M.E., Giavalisco, M., Steidel, C.C. & Fruchter, A., 1996, MNRAS, 283, 1388

Magdziarz P. & Zdziarski, A.A., 1995, MNRAS, 273, 837

Maggorian, J. et al., 1998, AJ, 115, 2285

Maiolino, R. & Rieke, G.H., 1995, ApJ, 454, 94

Maiolino, R., et al., 2003, MNRAS, 344, L59

Martínez-Sansigre, A., Rawlings, S., Lacy, M., Fadda, D., Marleau, F.R., Simpson, C., Wilott, C.J. & Jarvis, M.J., 2005, Nature, 436, 666

Matt, G., Pompilio, F. & La Franca, F., 1999, New A, 4, 191

McLeod, K.K. & Rieke, G.H., 1995, ApJ, 441, 96

Merloni, A., 2004, MNRAS, 353, 1035

Mihos, J.C. & Hernquist, L., 1994, ApJ, 425, L13

Morrison, R. & McCammon, D., 1983, ApJ, 270, 119

Murray, N., Quataert, E. & Thompson, T.A., 2005, ApJ, 618, 569

Mushotzky, R.F., Done, C. & Pounds, K.A., 1993, ARA&A, 31, 717

Mushotzky, R.F., Cowie, L.L., Barger, A.J. & Arnaud, K.A., 2000, Nature, 404, 459

Panessa, F. & Bassani, L., 2002, A&A, 394, 435

Perola, G.C., et al., 2004, A&A, 421, 491

Pompilio, F., La Franca, F. & Matt, G., 2000, A&A, 353, 440

Rigby, J.R., Rieke, G.H., Pérez-González, P.G., Donley, J.L., Alonso-Herrero, A., Huang, J.-S., Barmby, P. & Fazio, G.G., 2005, ApJ, 627, 134

Risaliti, G., Maiolino, R. & Salvati, M., 1999, ApJ, 522, 157

Risaliti, G., Elvis, M. & Nicastro, F., 2002, ApJ, 571, 234

Risaliti, G., Elvis, M., Fabbiano, G., Baldi, A. & Zezas, A., 2005, ApJ, 623, L93

Rosati, P., et al., 2002, ApJ, 566, 667

Schmitt, H.R., 2001, AJ, 122, 2243

Setti, G. & Woltjer, L., 1989, A&A, 224, L21

Shemmer, O., Brandt, W.N., Vignali, C., Schneider, D.P., Fan, X., Richards, G.T. & Strauss, M.A., 2005, ApJ, 630, 729

Silk, J. & Rees, M.J., 1998, A&A, 331, L1

Simpson, C., 2005, MNRAS, 360, 565

Spergel, D.N., et al., 2003, ApJS, 148, 175

Szokoly, G.P., et al., 2004, ApJS, 155, 271

Tamura, N., Ohta, K. & Ueda, Y., 2006, MNRAS, 365, 134

Thompson, T.A., Quataert, E. & Murray, N., 2005, ApJ, 630, 167

Tozzi, P. et al., 2001, ApJ, 562, 42

Treister, E. & Urry, C.M., 2005, ApJ, 630, 115

Treister, E. et al., 2004, ApJ, 616, 123

Tremaine, S., et al., 2002, ApJ, 574, 740

Ueda, Y., Akiyama, M., Ohta, K. & Miyaji, T., 2003, ApJ, 598, 886

Waskett, T.J., Eales, S.A., Gear, W.K., McCracken, H.J., Lilly, S & Brodwin, M., 2005, MNRAS, 363, 801

Wolf, C., et al., 2005, ApJ, 630, 771

Worsley, M.A., Fabian, A.C., Bauer, F.E., Alexander, D.M., Hasinger, G., Mateos, S., Brunner, H., Brandt, W.N. & Schneider, D.P., 2005, MNRAS, 357, 1281

Wyithe, J.S.B. & Loeb, A., 2003, ApJ, 595, 614

Zheng, W. et al., 2004, ApJS, 155, 73

Table 1. Results Assuming Both z and L_X Evolution

R_0	α	β	χ^2	P_{χ^2}	Γ_{1-10}	$\Gamma_{1-10}^{\rm Risaliti}$
$f_1 = K \exp\left(\frac{L_X}{10^{\beta}(1+z)^{\alpha}}\right)$						
1	14.9	42.5	215	6×10^{-40}	1.574	1.578
2	12.2	42.5	70.9	8×10^{-11}	1.505	1.505
3	11.1	42.5	31.8	8×10^{-4}	1.463	1.460
4	5.4	43	18.4	0.072	1.501	1.504
5	5.1	43	11.4	0.41	1.487	1.489
6	4.9	43	9	0.62	1.474	1.476
7	4.8	43	8.8	0.64	1.461	1.462
8	5.1	42.9	9.5	0.58	1.453	1.452
9	5	42.9	10.5	0.49	1.446	1.444
10	4.9	42.9	11.7	0.39	1.440	1.438
$f_1 = K(1+z)^{-\alpha}\left(\frac{L_X}{10^{41.5}}\right)^{\beta}$						
1	3.5	0.25	15.3	0.17	1.477	1.473
2	3	0.3	11.6	0.39	1.489	1.488
3	2.6	0.33	9.6	0.57	1.50	1.501
4	2.3	0.36	8.3	0.69	1.516	1.519
5	2.1	0.38	7.5	0.76	1.52	1.525
6	1.9	0.39	7.0	0.8	1.52	1.525
7	1.7	0.39	6.7	0.82	1.513	1.519
8	1.5	0.4	6.5	0.84	1.521	1.528
9	1.4	0.41	6.3	0.85	1.521	1.528
10	1.3	0.42	6.3	0.85	1.523	1.530
$f_2 = K(1+z)^{\alpha}(\log L_X)^{-\beta}$						
1	0.9	1.3	28.4	2.8×10^{-3}	1.412	1.402
2	0.5	2.7	18.4	0.072	1.407	1.398

Table 1—Continued

R_0	α	β	χ^2	P_{χ^2}	Γ_{1-10}	$\Gamma_{1-10}^{\rm Risaliti}$
3	0.4	4.7	15.2	0.18	1.423	1.419
4	0.3	4.8	13.8	0.24	1.418	1.413
5	0.3	6.3	13.1	0.29	1.434	1.432
6	0.2	5.1	12.7	0.32	1.415	1.411
7	0.2	5.9	12.2	0.35	1.425	1.422
8	0.2	6.5	11.9	0.37	1.431	1.429
9	0.2	6.9	11.8	0.38	1.434	1.433
10	0.2	7.3	11.7	0.39	1.439	1.438
$f_2 = K(1+z)^\alpha \cos^2\left(\frac{\log L_X - 41.5}{\beta}\right)$						
1	0.9	5.5	25.0	9×10^{-3}	1.467	1.465
2	0.5	4.4	13.8	0.24	1.474	1.475
3	0.3	4.4	11.2	0.43	1.466	1.468
4	0.2	4.3	10.1	0.52	1.465	1.467
5	0.2	3.8	8.9	0.63	1.480	1.484
6	0.1	4.2	9.1	0.61	1.461	1.464
7	0.1	3.9	8.3	0.69	1.472	1.476
8	0.1	3.7	8.1	0.70	1.481	1.486
9	0.1	3.6	8.2	0.69	1.484	1.490
10	0.1	3.5	8.5	0.67	1.489	1.495

Note. — P_{χ^2} is the null-hypothesis probability for the calculated χ^2. Γ_{1-10} is the photon-index between 1 and 10 keV of the CXRB spectrum predicted by that particular model. $\Gamma_{1-10}^{\rm Risaliti}$ is the photon-index when the Risaliti et al. (1999) $N_{\rm H}$ distribution is used.

Table 2. Results Assuming only L_X Evolution

R_0	β	χ^2	P_{χ^2}
$f_1 = K \exp\left(\frac{L_X}{10^\beta}\right)$			
1	46.9	279	10^{-52}
2	44.8	96	4×10^{-15}
3	44.6	43.3	2×10^{-5}
4	44.6	24.8	0.016
5	44.5	17.8	0.12
6	44.5	15.8	0.20
7	44.4	15.8	0.20
8	44.4	16.4	0.18
9	44.4	17.5	0.13
10	44.4	19.0	0.088
$f_1 = K \left(\frac{L_X}{10^{41.5}}\right)^\beta$			
1	0.0	279	10^{-52}
2	0.0	97	2×10^{-15}
3	0.0	46.4	6×10^{-6}
4	0.0	29.1	3.8×10^{-3}
5	0.01	23.0	0.028
6	0.08	19.6	0.076
7	0.14	16.7	0.16
8	0.18	14.4	0.27
9	0.21	12.6	0.40
10	0.24	11.2	0.51
$f_2 = K(\log L_X)^{-\beta}$			
1	0.0	279	10^{-52}
2	0.0	97	2×10^{-15}

Table 2—Continued

R_0	β	χ^2	P_{χ^2}
3	0.0	46.4	6×10^{-6}
4	0.0	29.1	3.8×10^{-3}
5	0.1	23.0	0.028
6	1.0	20.2	0.063
7	1.7	18.4	0.10
8	2.2	17.2	0.14
9	2.7	16.2	0.18
10	3.0	15.5	0.21
$f_2 = K \cos^2\left(\frac{\log L_X - 41.5}{\beta}\right)$			
1	39.9	280	8×10^{-53}
2	39.9	97	2×10^{-15}
3	39.9	46.5	6×10^{-6}
4	9.7	28.6	4.5×10^{-3}
5	6.3	20.1	0.065
6	5.3	15.5	0.22
7	4.8	12.7	0.39
8	4.5	11.0	0.53
9	4.3	9.9	0.62
10	4.1	9.2	0.69

Note. — P_{χ^2} is the null-hypothesis probability for the calculated χ^2. Here, the number of degrees of freedom is 12.

Table 3. Results Assuming Luminosity-Dependent z Evolution

R_0	$\alpha_{41.5}$	$\alpha_{43.5}$	β	χ^2	P_{χ^2}
$f_1 = K \exp\left(\frac{L_X}{10^{\beta}(1+z)^{\alpha(L_X)}}\right)$					
1	14.9	17.9	42	120	1.7×10^{-20}
2	12.2	16.1	42	38.7	5.9×10^{-5}
3	11.1	15.2	42	19.5	0.052
4	5.4	14	42	14.5	0.21
5	5.1	5.1	43	11.4	0.41
6	4.9	4.9	43	9	0.62
7	4.8	4.8	43	8.8	0.64
8	5.1	5.1	42.9	9.5	0.58
9	5	5	42.9	10.5	0.49
10	4.9	4.9	42.9	11.7	0.39
$f_1 = K(1+z)^{-\alpha(L_X)} \left(\frac{L_X}{10^{41.5}}\right)^{\beta}$					
1	3.5	1.0	0.0	10.6	0.48
2	3	1.0	0.09	9.0	0.63
3	2.6	1.2	0.18	8.1	0.70
4	2.3	1.3	0.24	7.6	0.75
5	2.1	1.5	0.31	7.1	0.79
6	1.9	1.5	0.34	6.8	0.81
7	1.7	1.5	0.37	6.6	0.83
8	1.5	1.6	0.41	6.5	0.84
9	1.4	1.5	0.42	6.3	0.85
10	1.3	1.6	0.45	6.2	0.86
$f_2 = K(1+z)^{\alpha(L_X)}(\log L_X)^{-\beta}$					
1	0.9	0.8	0.0	2.5	4.7×10^{-3}
2	0.5	0.3	0.2	17.1	0.11

Table 3—Continued

R_0	$\alpha_{41.5}$	$\alpha_{43.5}$	β	χ^2	P_{χ^2}
3	0.4	0.0	0.0	13.5	0.26
4	0.3	0.0	1.1	12.9	0.30
5	0.3	0.0	2.6	11.9	0.37
6	0.2	0.0	2.7	12.4	0.34
7	0.2	0.0	3.4	11.8	0.38
8	0.2	0.0	4.0	11.4	0.41
9	0.2	0.0	4.5	11.2	0.43
10	0.2	0.0	4.8	11.1	0.44
$f_2 = K(1+z)^{\alpha(L_X)} \cos^2\left(\frac{\log L_X - 41.5}{\beta}\right)$					
1	0.9	0.9	5.5	25.0	9×10^{-3}
2	0.5	0.5	4.4	13.8	0.24
3	0.3	0.4	3.9	10.5	0.49
4	0.2	0.4	3.4	9.1	0.61
5	0.2	0.2	3.8	8.9	0.63
6	0.1	0.3	3.3	8.0	0.71
7	0.1	0.2	3.5	8.0	0.71
8	0.1	0.1	3.7	8.1	0.70
9	0.1	0.1	3.6	8.2	0.69
10	0.1	0.0	3.9	8.3	0.69

Note. — P_{χ^2} is the null-hypothesis probability for the calculated χ^2. $\alpha_{41.5}$ is the value of $\alpha(L_X)$ at $\log L_X = 41.5$. $\alpha_{43.5}$ is the value of $\alpha(L_X)$ at $\log L_X = 43.5$

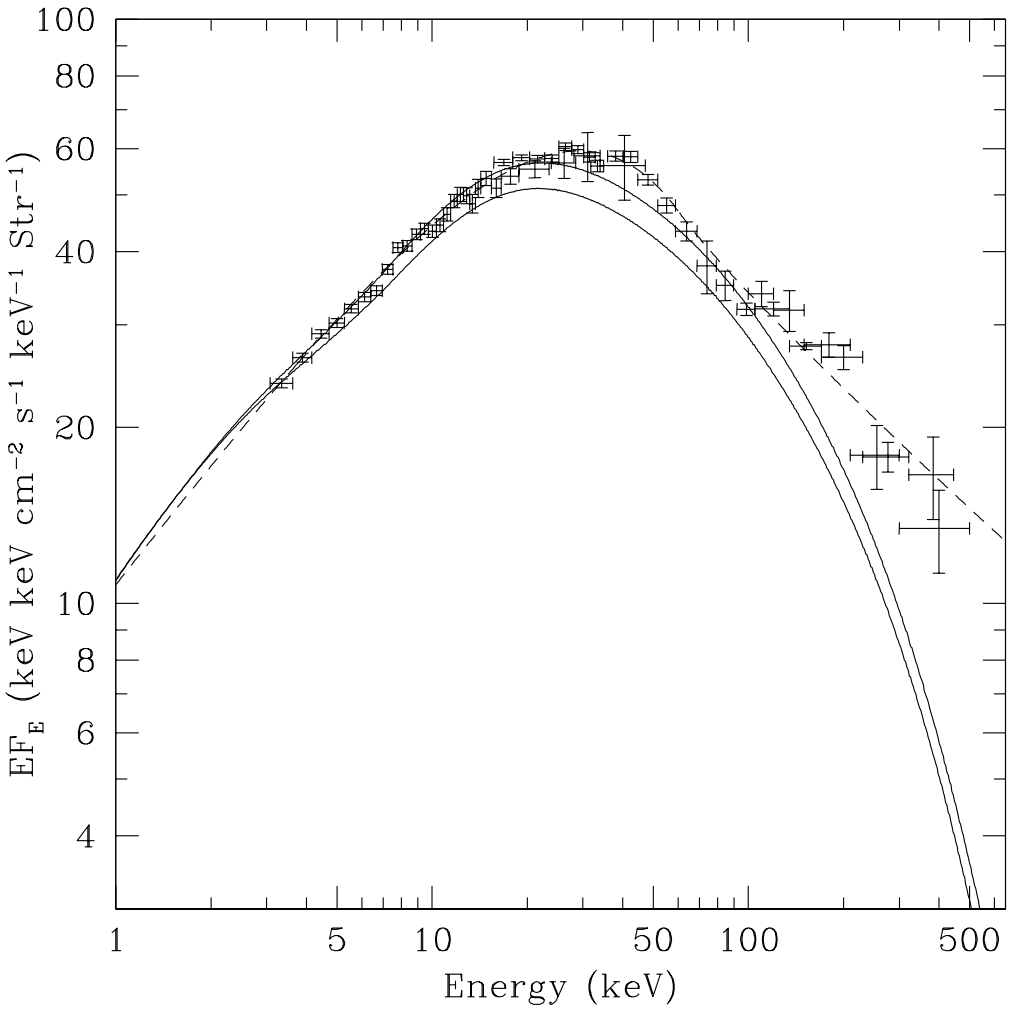

Fig. 1.— The CXRB spectrum between 1 and 600 keV. The data points are from the HEAO-1 experiment (Gruber et al. 1999), shifted upwards by 40% to more closely match newer measurements (De Luca & Molendi 2004). The dashed line is the analytical fit to the HEAO-1 data provided by Gruber et al. (1999). It has also been shifted upwards by 40%. The upper solid curve is a model of the CXRB produced using the same parameters as Treister & Urry (2005). The major differences from our model are a reflection fraction of 2, a high-energy cutoff of 300 keV and a constant $R = 3$ for all L_X and z. The lower solid curve is identical to the previous one except that the effects of Compton-thick absorbers are properly included. This has an important effect on the shape of the spectrum, particularly around the peak of the intensity at 20–40 keV. Both curves have had their normalizations increased by a factor of 1.5 to match the data at low energy.

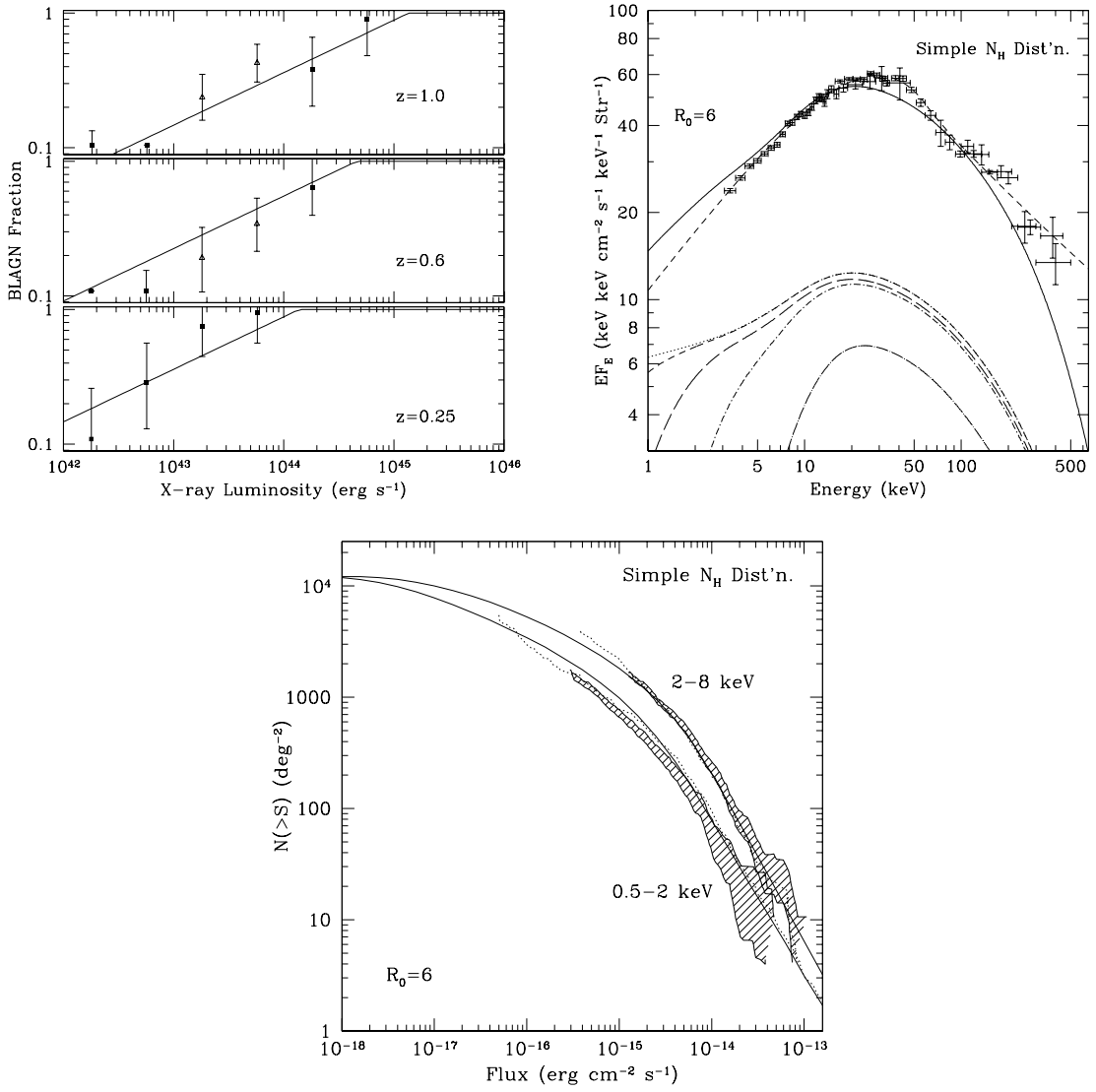

Fig. 2.— Results from the power-law parameterization (Eq. 8) when $R_0 = 6$. *(Upper-left panel)* The solid line plots the predicted fraction of Type 1 or broad-line AGNs (BLAGNs) at $z = 0.25, 0.6$ and 1.0. The points are the observed values from Barger et al. (2005). Open triangles represent sources which contribute the majority of the CXRB (Ueda et al. 2003; Barger et al. 2005). This particular parameterization is an extremely good fit to the Barger data with $P_{\chi^2} = 0.8$. *(Upper-right panel)* The CXRB spectrum predicted by this evolutionary model. The lines and points are as in Fig. 1. In addition, the contribution from sources with $\log N_{\rm H} = 20 - 21$ (dotted line), $21 - 22$ (short dashed line), $22 - 23$ (long dashed line), $23 - 24$ (dot-short dashed line), and $24 - 24.5$ (dot-long dashed line) are also plotted. *(Lower Panel)* The solid lines show the predictions for the 0.5–2 keV and 2–8 keV X-ray number counts using this parameterization for the AGN Type 2/Type 1 ratio. The hatched regions are the observed distributions from the Extended *Chandra* Deep Field South (Lehmer et al. 2005). The dotted line in the 2–8 keV band is from the *Chandra* Deep Field South (Rosati et al. 2002), while the dotted line in the 0.5–2 keV band is from Hasinger et al. (2005).

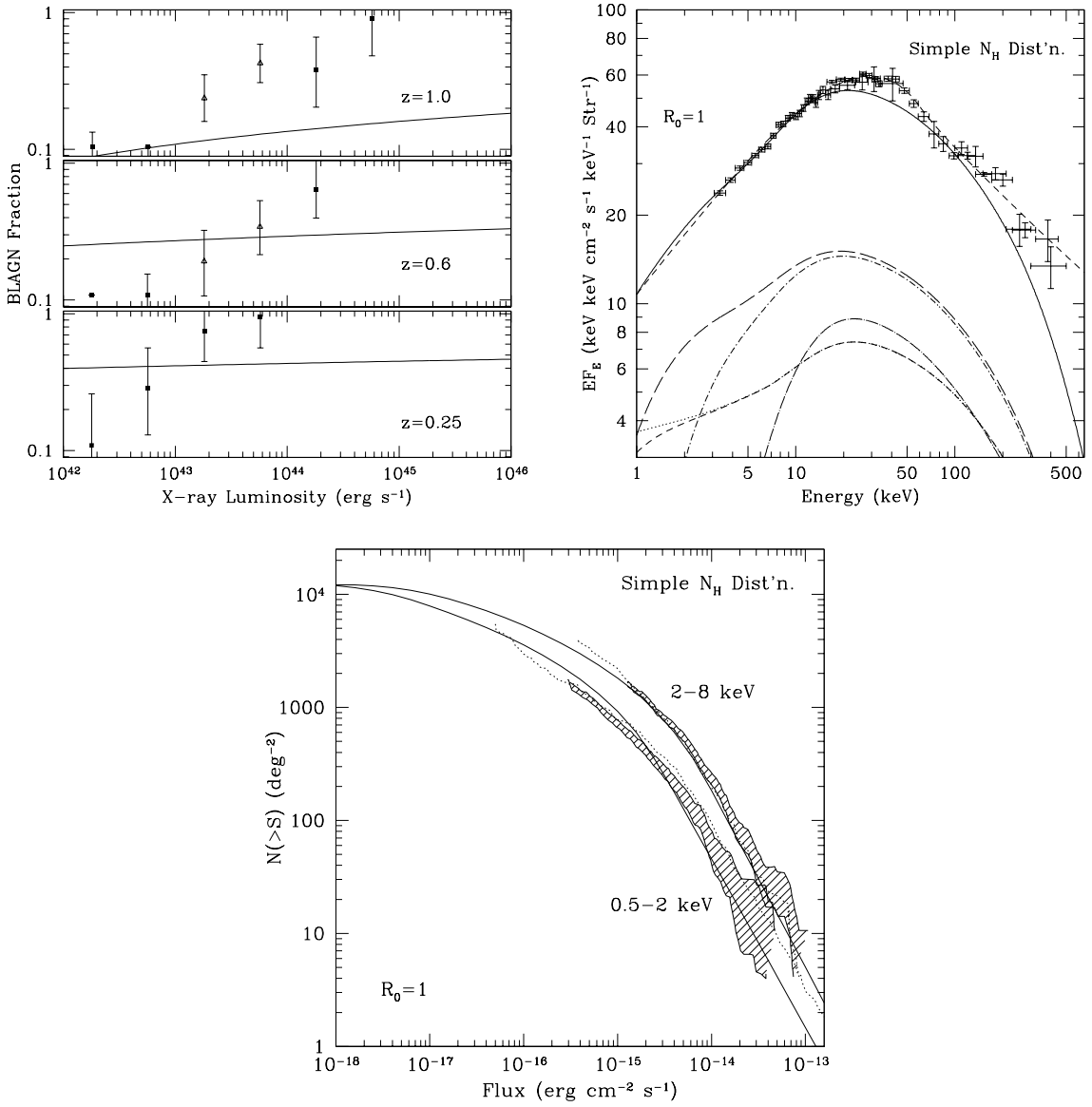

Fig. 3.— Results from the $\log L_X$ power-law parameterization (Eq. 9) when $R_0 = 1$. Plots are as in Fig. 2. The fit to the Barger data is poor with $P_{\chi^2} = 2.8 \times 10^{-3}$.

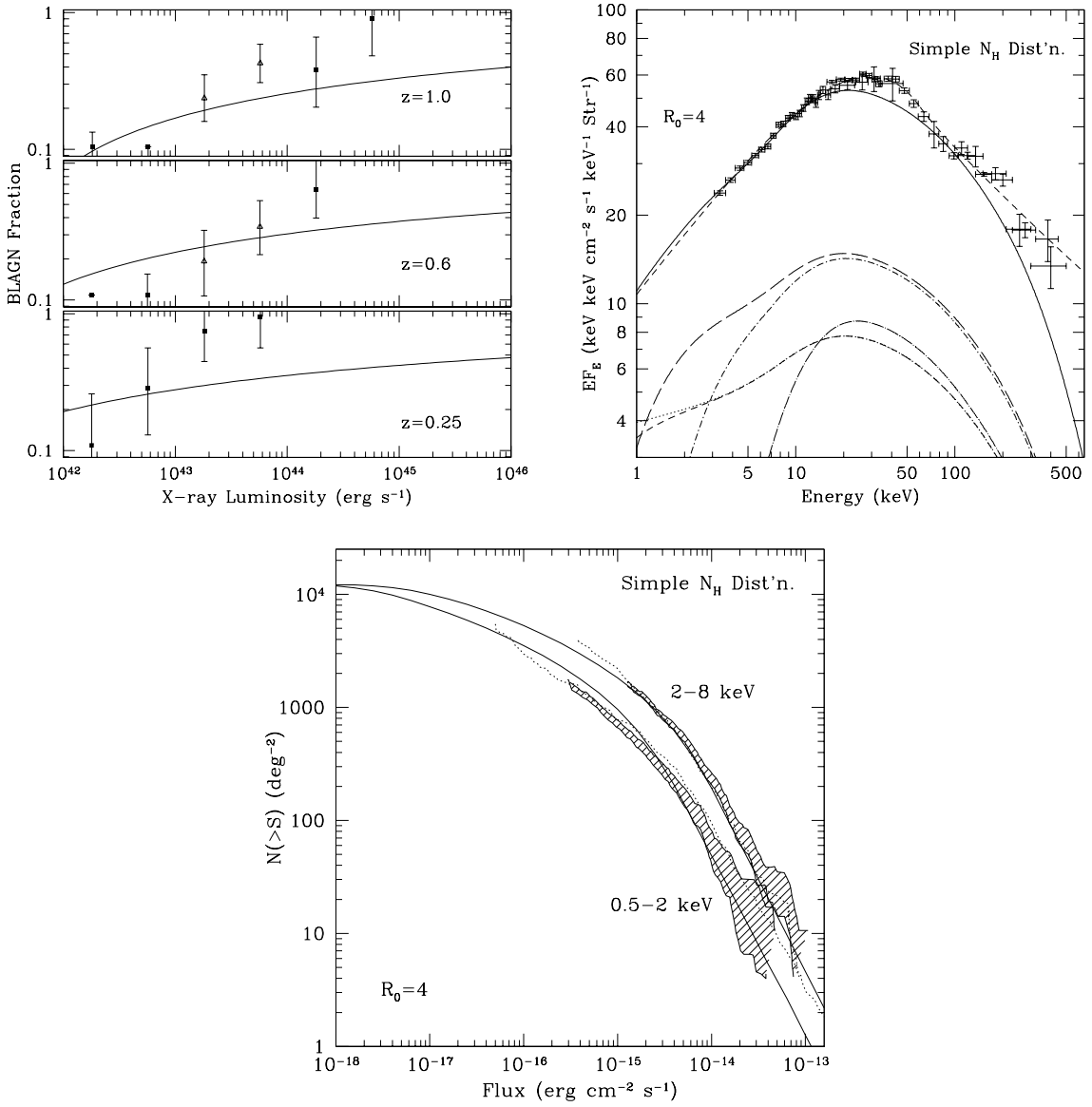

Fig. 4.— Results from the $\log L_X$ power-law parameterization (Eq. 9) when $R_0 = 4$. Plots are as in Fig. 2. The fit to the Barger data has a $P_{\chi^2} = 0.24$.

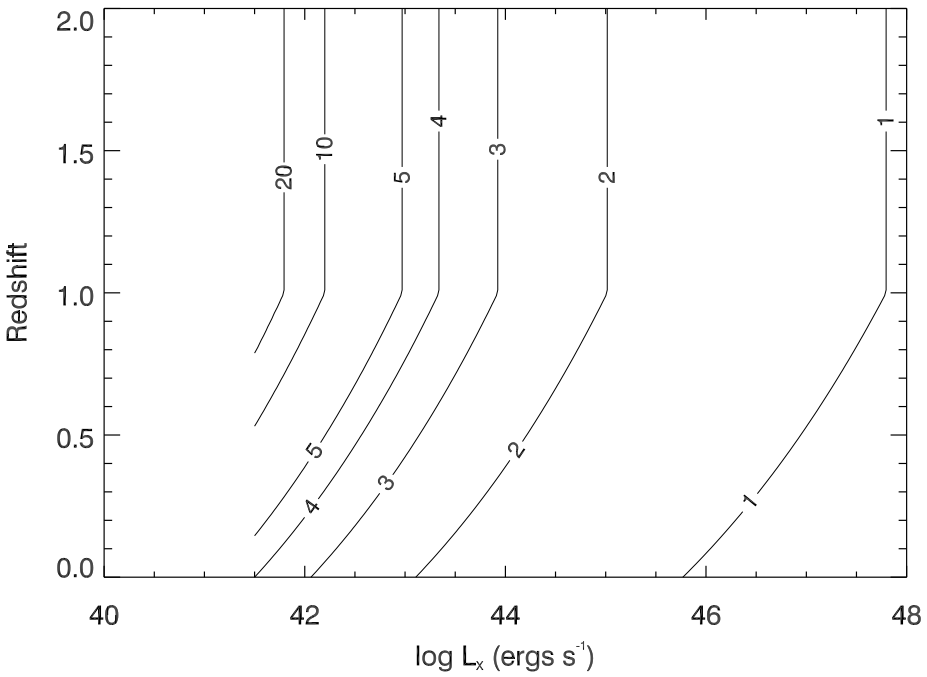

Fig. 5.— A contour plot of R, the AGN Type 2/Type 1 ratio, as a function of $\log L_X$ and z predicted from the $R_0 = 4$ model of Eq. 9 (Fig. 4). Recall that the evolution in redshift was halted at $z = 1$.

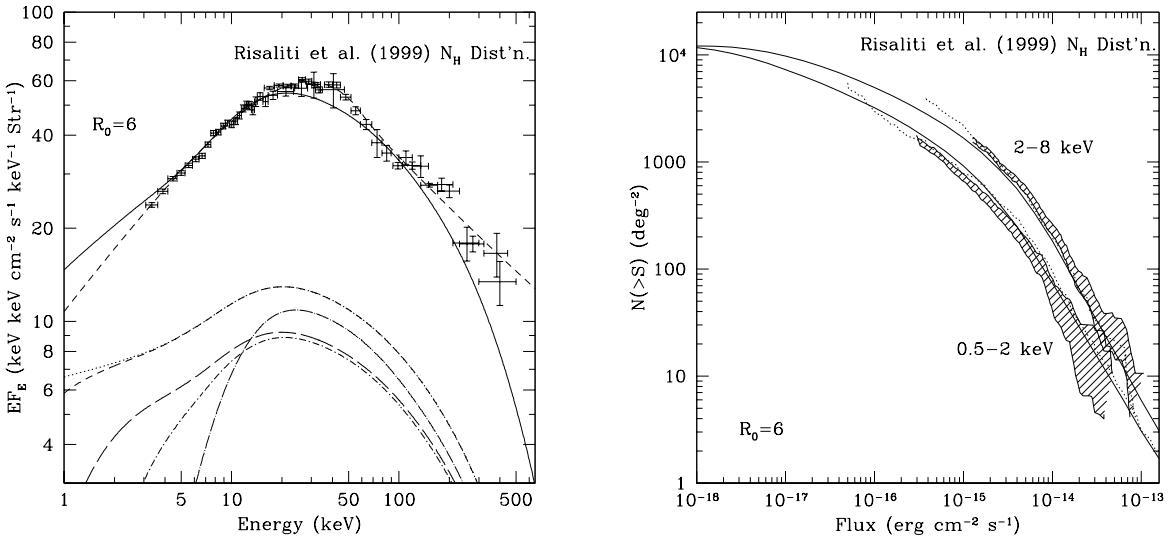

Fig. 6.— Results from the power-law parameterization (Eq. 8) when $R_0 = 6$ (as in Fig. 2) except the Risaliti et al. (1999) $N_{\rm H}$ distribution is assumed. The model spectra were multiplied by a factor of 1.57.

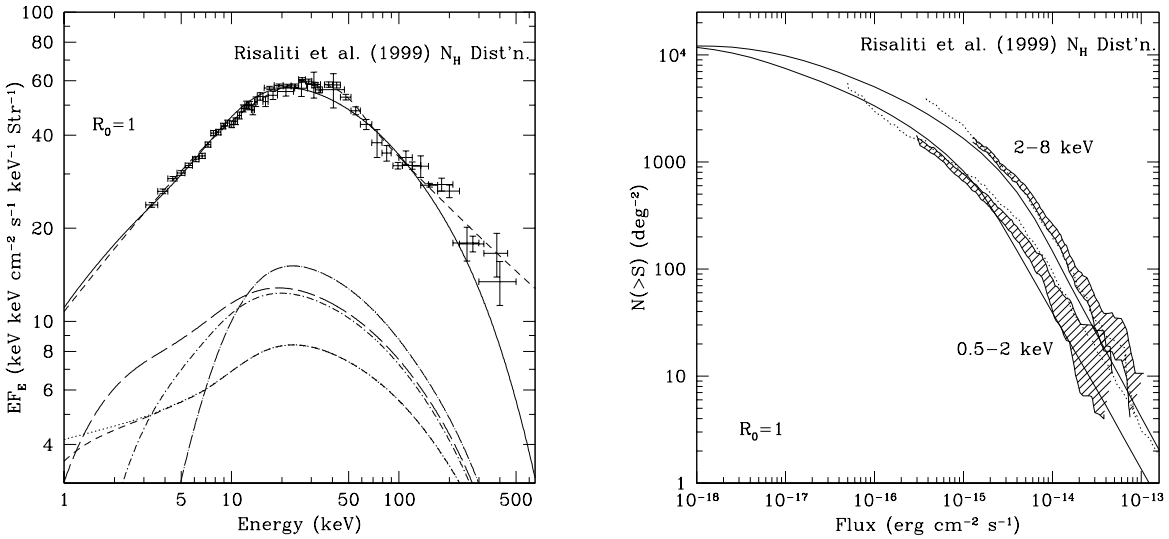

Fig. 7.— Results from the $\log L_X$ power-law parameterization (Eq. 9) when $R_0 = 1$ (as in Fig. 3) except the Risaliti et al. (1999) $N_{\rm H}$ distribution is assumed. The model spectra were multiplied by a factor of 1.7.

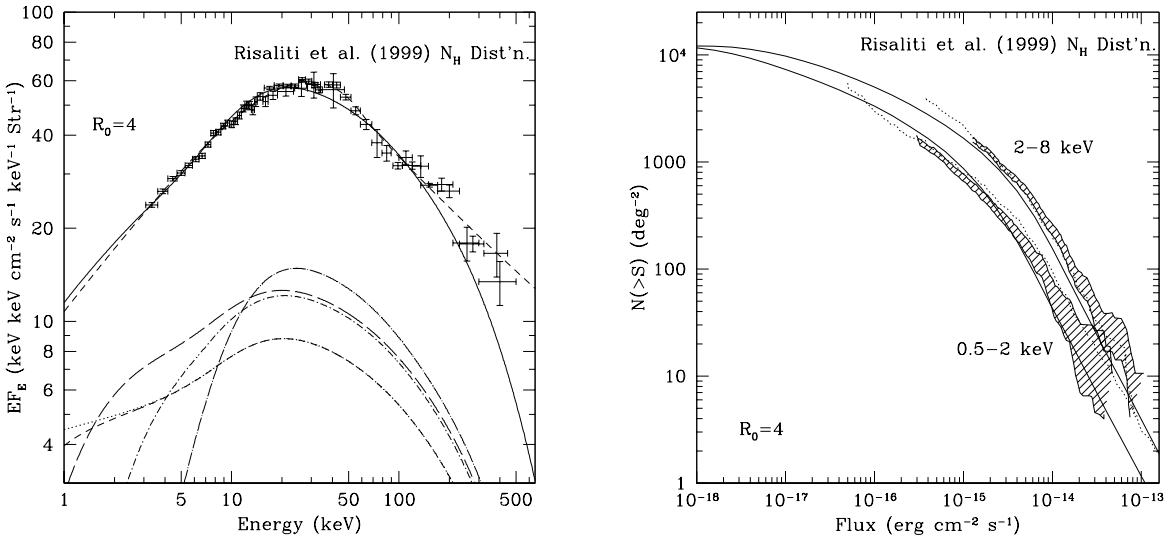

Fig. 8.— Results from the $\log L_X$ power-law parameterization (Eq. 9) when $R_0 = 4$ (as in Fig. 4) except the Risaliti et al. (1999) $N_{\rm H}$ distribution is assumed. The model spectra were multiplied by a factor of 1.7.